Textural Features Sensitivity to Scale and Illumination Variations

Pavel Vácha[1] and Michal Haindl[1,2(✉)]

[1] The Institute of Information Theory and Automation of the ASCR, Prague, Czechia
{vacha,haindl}@utia.cas.cz
[2] Faculty of Management, University of Economics, Jindřichuv Hradec, Czechia
http://www.utia.cas.cz

Abstract. Visual scene recognition is predominantly based on visual textures representing an object's material properties. However, the single material texture varies in scale and illumination angles due to mapping an object's shape. We present a comparative study of the color histogram, Gabor, opponent Gabor, Local Binary Pattern (LBP), and wide-sense Markovian textural features concerning their sensitivity to simultaneous scale and illumination variations. Due to their application dominance, these textural features are selected from more than 50 published textural features. Markovian features are information preserving, and we demonstrate their superior performance for scale and illumination variable observation conditions over the standard alternative textural features. We bound the scale variation by double size, and illumination variation includes illumination spectra, acquisition devices, and 35 illumination directions spanned above a sample.

Keywords: Markovian textural features · LBP · Gabor features · Scale sensitivity · Illumination sensitivity

1 Introduction

A human observer recognizes a visual scene using shape and material attributes. Unfortunately, the surface material's appearance vastly changes under variable observation conditions, negatively affecting its automatic and reliable recognition in numerous artificial intelligence applications. As a consequence, most material recognition attempts apply unnaturally restricted observation conditions [2,6,37]. Modeled Scale Invariant Feature Transform (SIFT) features using Johnson distribution [18] allow features invariant in rotation, scale, and illumination. Authors [29] proposed fractal dimension calculated in the Gaussian scale-space texture representation. Fractal images combined with LBP images using an indexing function to obtain scale-invariant features. Galois field-based features in [31] were used for rotation and scale invariant texture classification.

The Czech Science Foundation project GAČR 19-12340S supported this research.

C. Bădică et al. (Eds.): ICCCI 2022, CCIS 1653, pp. 237–249, 2022.
https://doi.org/10.1007/978-3-031-16210-7_19

Rotation, scale, and illumination invariant features [39] use LBP and log-polar energy-based descriptors in the dual-tree complex wavelet transform domain. Another rotation, illumination, and scale invariance variant of LBP (IRSLBP) was published in [38], where partial scale invariance authors achieved using three different neighborhood radii. Although over 50 various textural features were published [23,33], we restricted our comparison to the most effective and thus dominant textural features. An ideal model for representing and classifying materials should be capable of capturing fundamental perceptual materials properties. A multi-dimensional visual texture is an appropriate paradigm for such a surface reflectance function model. The best measurable representation is the seven-dimensional Bidirectional Texture Function (BTF) [10]. BTF can be simultaneously measured, even if it is not a trivial task, modeled using state-of-the-art measurement devices and computers and the most advanced visual data mathematical models. Features derived from such multi-dimensional data models are information preserving because they can synthesize data spaces resembling the original measurement data space. The authors have introduced a family of fast multi-resolution Markov random field-based models. They have shown that these models excel in robustness to illumination conditions [14].

This paper's contribution is a joint test of scale and illumination variations to simulate realistic visual scene recognition conditions and we present a comparative analysis with several most common alternative textural features representing four alternatives most commonly used textural features. For this analysis, we take advantage of the unique UTIA BTF visual material measurements [13].

2 Markovian Textural Features

The texture is factorized into K levels of the Gaussian down-sampled pyramid and subsequently each pyramid level is modeled by a wide-sense Markovian type of model - the Causal Auto-regressive Random (CAR) model. Let us assume that each multispectral (color) texture is composed of C spectral planes (usually $C = 3$), $Y_r = [Y_{r,1}, \ldots, Y_{r,C}]^T$ is the multispectral pixel at location r. The multiindex $r = (r_1, r_2)$ is composed of row index r_1 and column index r_2. The spectral planes are mutually decorrelated by the Karhunen-Loéve transformation. The two-dimensional models assume that the j-th spectral plane of the pixel at position r can be modeled as:

$$Y_{r,j} = \gamma_j Z_{r,j} + \epsilon_r \ , \tag{1}$$

where $Z_{r,j} = [Y_{r-s,j} : \forall s \in I_r]^T$ is the $\eta \times 1$ data vector, ϵ_r is Gaussian white noise with constant but unknown variance, $\gamma_j = [a_{1,j}, \ldots, a_{\eta,j}]$ is the $1 \times \eta$ unknown parameter vector. Some selected contextual causal or unilateral neighbor index shift set is denoted I_r and $\eta = cardinality(I_r)$, see Fig. 1. The texture is analyzed in a chosen direction, where multi-index t changes according

to the movement on the image lattice I. Given the known CAR process history $Y^{(t-1),j} = \{Y_{t-1,j}, Y_{t-2,j}, \ldots, Y_{1,j}, Z_{t,j}, Z_{t-1,j}, \ldots, Z_{1,j}\}$, $\hat{\gamma}_j$ can be estimated using fast, numerically robust recursive statistics [9]:

$$V_{t-1,j} = \begin{pmatrix} \sum_{u=1}^{t-1} Y_{u,j} {Y_{u,j}}^T & \sum_{u=1}^{t-1} Y_{u,j} {Z_{u,j}}^T \\ \sum_{u=1}^{t-1} Z_{u,j} {Y_{u,j}}^T & \sum_{u=1}^{t-1} Z_{u,j} {Z_{u,j}}^T \end{pmatrix} + V_0 = \begin{pmatrix} V_{y,j(t-1)} & V_{zy,j(t-1)}^T \\ V_{zy,j(t-1)} & V_{z,j(t-1)} \end{pmatrix} \quad (2)$$

$$\hat{\gamma}_{t-1,j}^T = V_{z,j(t-1)}^{-1} V_{zy,j(t-1)} \ , \quad (3)$$

$$\lambda_{t-1,j} = V_{y,j(t-1)} - V_{zy,j(t-1)}^T V_{z,j(t-1)}^{-1} V_{zy,j(t-1)} \ , \quad (4)$$

where the positive definite matrix V_0 represents prior knowledge. Our textural features are $a_{s,j}\ \forall s \in I_r, j = 1, \ldots, C$ which are color invariants and additional color invariant features derived from this model in [15]. The spectral index is excluded for simplification in (10)–(20) for all statistics in these invariants.

$$\alpha_3 = \sqrt{\sum_{\forall r \in I} \left(Y_r - \hat{\gamma}_t Z_r\right)^T \lambda_t^{-1} \left(Y_r - \hat{\gamma}_t Z_r\right)} \ , \quad (5)$$

$$\alpha_4 = \sqrt{\sum_{\forall r \in I} \left(Y_r - \mu\right)^T \lambda_t^{-1} \left(Y_r - \mu\right)} \ \} \ , \quad (6)$$

$$\beta_6 = \ln \left(\sum_{\forall r \in I} \frac{1}{|I|} \ p\left(Y_r | Y^{(r-1)}\right) \left|V_{y(t)}\right|^{\frac{1}{2}} \right) \ , \quad (7)$$

$$\beta_7 = \ln \left(\ln p\left(Y^{(t)} | M\right) \ + \ (\psi(t+1) + 2) \ln \left|V_{y(t)}\right| \right) \ , \quad (8)$$

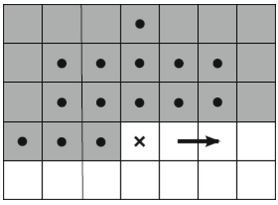

Fig. 1. Unilateral contextual neighborhood I_r of sixth-order used for CAR model. X marks the current pixel, the bullets are pixels in the neighborhood, the arrow shows movement direction, and the grey area indicates acceptable neighborhood pixels. (Color figure online)

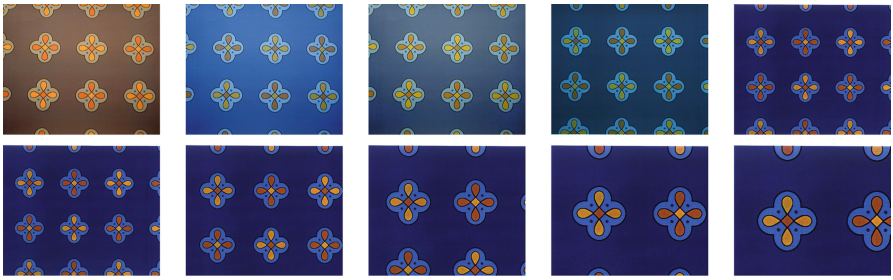

Fig. 2. The appearance of patterns from the UEA database with varying illumination spectra, acquisition devices (top row), and scale (bottom row).

$$\alpha_1 = \sum_{j=1}^{C} a_{i,j} \quad \forall i \ , \tag{9}$$

$$\alpha_2 = 1 + Z_t^T \, V_{z(t)}^{-1} \, Z_t \ , \tag{10}$$

$$\beta_1 = \ln\left(\frac{\psi(r)}{\psi(t)} \left|\lambda_t\right| \left|\lambda_r\right|^{-1}\right) \ , \tag{11}$$

$$\beta_2 = \ln\left(\frac{\psi(r)}{\psi(t)} \left|V_{z(t)}\right| \left|V_{z(r)}\right|^{-1}\right) \tag{12}$$

$$\beta_3 = \ln\left(\left|V_{z(t)}\right| \left|\lambda_t\right|^{-\eta}\right) \ , \tag{13}$$

$$\beta_4 = \ln\left(\left|V_{z(t)}\right| \left|V_{y(t)}\right|^{-\eta}\right) \ , \tag{14}$$

$$\beta_5 = \operatorname{tr}\left\{V_{y(t)} \ \lambda_t^{-1}\right\} \ , \tag{15}$$

$$\beta_8 = \left(\frac{\psi(r)}{\psi(t)} \left|\lambda_t\right| \left|\lambda_r\right|^{-1}\right)^{\frac{1}{2}} \ , \tag{16}$$

$$\beta_9 = \left(\frac{\psi(r)}{\psi(t)} \left|V_{z(t)}\right| \left|V_{z(r)}\right|^{-1}\right)^{\frac{1}{2\eta}} \tag{17}$$

$$\beta_{10} = \left(\left|V_{z(t)}\right| \left|\lambda_t\right|^{-\eta}\right)^{\frac{1}{2}} \ , \tag{18}$$

$$\beta_{11} = \left(\left|V_{z(t)}\right| \left|V_{y(t)}\right|^{-\eta}\right)^{\frac{1}{2}} \ , \tag{19}$$

$$\beta_{12} = \sqrt{\left|V_{y(t)}\right| \left|\lambda_t\right|^{-1}} \ , \tag{20}$$

where μ is the mean value of Y_r and $\psi(t)$ is a number of the pixel from the beginning. $p\left(Y^{(t)}|M\right)$ is the posterior probability of the model (1), and $p\left(Y_r|Y^{(r-1)}\right)$ is prediction probability, both defined in [9]. We used neigborhood I_r of sixth order (see Fig. 1), where $\eta = 14$, $r = 0$ coresponding to prior, and t equals to the last pixel in the image. All invariants (10)–(20) were computed on all spectral planes and concatenated into the feature vector. The CAR model and color invariant feature vector were computed on $K = 5$ Gaussian pyramid levels and in 3 directions, and the features were again concatenated. Finally, the feature vectors were compared with fuzzy contrast FC_3 [30]. Downscaling on the Gaussian pyramid is possible as the image provides sufficient resolution. It may be needed for lower resolution images to use $K = 4$ levels of the Gaussian pyramid, which was also tested. When the Karhunen-Loéve transformation preceded CAR features computation, they were denoted by the '-KL' suffix. The feature vector size is 1515 for $K = 5$ and 1212 for $K = 4$ pyramid levels.

3 Frequented Alternative Features

Hundreds of various textural features were published and to test all these features on the extensive UTIA BTF wood database (426 465 wood images, 260 TB of data) is infeasible. Hence, we compare the CAR features with the following most frequented four alternatives, each compared with their author's suggested distance:

- Color histogram features computed as cumulative histogram [34] on each spectral plane separately and concatenated, compared with L1 distance (384 features).
- Gabor features [7,16,21,25] computed on each spectral plane separately and concatenated, compared with L1 distance normalized to standard deviation of features (144 features).
- Opponent Gabor features [19] compared with L2 distance normalized to standard deviation of features (252 features).
- Local Binary Patterns $\mathrm{LBP}_{8,1+8,3}$ and $\mathrm{LBP}^{u}_{16,2}$ [27] computed either on grayscale images or each spectral plane separately and concatenated, compared with the Kullback Leibler divergence (1536 and 243 features). LBP features exist in various modifications [1,5,17,20,22,26,40], but they have similar behavior; hence we chose two of their variants as representatives of the whole group as any comparison cannot be considered an exhaustive investigation without the LBP strategy.

The setup of listed features is described in more detail in [15]. The other tested parameters were under-performing, namely histogram and Gabor features on gray images. We excluded fashionable neural net features due to their uncompetitiveness on often restricted test data in practical applications. They are little understood, wasteful, dependent on the net topology, and thus cannot be regarded as well-defined textural features. Moreover, we use only between one to six training images which are insufficient for neural net robust learning. The MRF features outperformed deep CNN in the bark recognition problem even on extensive training data, as demonstrated in [28]. This result is understandable because MRF features are descriptive while neural net features are discriminative. Similar results were presented in the extensive comparison of the multilayer NN marble textures classification with 17 variants of the LBP feature and three types of key-point texture descriptors in [32]. In their results, the CNN features never outperform all these alternatives. Another comparison where NN - ScatNet, PCANet, FV-AlexNet, and RandNet do not outperform LBP features on Outex, CUReT, ALOT, and KTHTIPS data can be consulted in [24]. However, it would be interesting to include tests with a low number of training samples which would reveal the robustness of features to various conditions as in [3,36].

4 Experiments

We tested the scale sensitivity of the selected textural features on two databases:

Fig. 3. The appearance of two veneers from the Wood UTIA BTF database in varying illumination direction (upper two rows) and different scale (bottom row).

(i) University of East Anglia (UEA) Uncalibrated Image Database [4] consisting of patterns under different illumination spectra and
(ii) wooden BTF measurements from the extensive UTIA BTF database [13] composed of material images under varying illumination directions.

4.1 University of East Anglia Uncalibrated Image Database

The UEA dataset contains 28 textile designs, captured with six different devices (4 color cameras and two color scanners), and images for cameras were illuminated with three different illumination spectra, which sums up to 394 images in total (see examples in Fig. 2). UEA images are supposed to include even non-linear relations of images caused by different processing in acquisition devices (gamma correction) [4], no light calibration was performed. Since the UEA database images include some scale variations, we have corrected this and rescaled the images to have the same scale and resolution.

4.2 Wood UTIA BTF Database

This study's Wood UTIA BTF database contains veneers from sixty-five varied European, African, and American wood species. The UTIA BTF database[1] was measured using the high precision robotic gonioreflectometer [11], which consists of independently controlled arms with a camera and light. Its parameters, such as angular precision of 0.03°, the spatial resolution of 1000 DPI, or selective spatial measurement, classify this gonioreflectometer as a state-of-the-art device. They

[1] http://btf.utia.cas.cz/.

measured each wood sample in 81 viewing positions times 81 illumination positions resulting in 6561 images per sample, 4 TB of data. Because of substantial storage requirements, we took only images for one camera position (top view), and we selected 35 from 81 illumination directions (1 image with the tilt of 0°, 12 images with 30°, ten images with 60°, and 12 images with 75°). The images uniformly represent the space of possible illumination directions (examples in Fig. 3).

4.3 Setup

In both experiments, all images were scaled down to $95\%, 90\%, 85\%, \ldots, 50\%$ of their original size, and regions with the same resolution were cropped. Consequently, the image of scale 50% covers double the size of the original texture image, but with half of the details than scale 100%. The training set contains only images with original scales, and the classification accuracy was tested for all scales separately. Training images per each material were randomly selected from the training set, and the remaining images were classified using the Nearest Neighbor (1-NN) classifier. The number of training images went from 1 to 6, and the results averaged over 10^3 of random selections of training images. Even single training samples were randomly selected, so they could have different illumination conditions for each material, making recognition more challenging. In total, we used 4 312 images with 332×275 resolution for UEA and 25 025 images with 816×802 resolution for Wood UTIA BTF.

Table 1. Classification accuracy [%] averaged over all scales and illumination angles on the UEA/Wood UTIA BTF datasets. Columns display results for the increasing number of training samples per class.

	UEA			Wood UTIA BTF		
No. of training samples	1	3	6	1	3	6
Color histogram	15.3	23.2	32.6	10.6	19.7	28.6
Gabor	33.9	46.2	59.7	18.0	28.6	36.8
Opponent Gabor	44.0	61.0	70.1	24.0	36.4	44.3
$\mathrm{LBP}^{u}_{16,2}$, gray	18.4	35.0	45.8	7.2	11.0	13.3
$\mathrm{LBP}_{8,1+8,3}$, color	14.1	28.2	38.1	13.3	21.0	25.6
2D CAR-KL ($K = 4$)	43.1	58.2	67.0	39.9	55.7	64.3
2D CAR-KL	48.4	62.8	70.2	**45.4**	**61.4**	**69.4**
2D CAR	**52.1**	**66.2**	**73.0**	32.8	47.1	55.7

4.4 Results

Table 1 summarizes recognition accuracy for the best parameters of compared features. The 2D CAR features are superior for all test numbers of random training images per material. The classification of the accuracy of 2D CAR-KL averaged over all scale variations goes from 48.4%/45.4% (UEA/Wood UTIA BTF)

for one training sample to 70.2%/69.4% for six training samples per class. The standard deviation is less than 4 for one training sample, less than 3 for six training samples for UEA, and less the 2 for Wood UTIA BTF for all features. The 2D CAR model achieved slightly better results without the Karhunen-Loève transformation for UEA. However, we include 2D CAR-KL for more detailed analysis since it has better classification accuracy for other experiments [14]. Also, the 2D CAR-KL model on $K = 4$, levels of the Gaussian pyramid achieved lower accuracy than the standard $K = 5$ levels if the images have sufficient resolution (Wood UTIA BTF). The only comparable features for UEA are opponent Gabor features that achieved similar performance as 2D CAR-KL with slightly lower accuracy for one training sample. Gabor features are also the best alternative in Wood UTIA BTF, but their accuracy is more than 20% points lower than 2D CAR-KL. Color histograms suffer from their sensitivity to color changes, which results in their low performance. Even though the color histograms are robust to scale variation (because they do not describe spatial relations) they are unable to recognize materials under different illumination spectra. LBP and histogram features did not perform satisfactorily. The reason is that binarized LBP micropatterns are sensitive to illumination direction [35]. They are also very sensitive to even slight scale variations, as confirmed by [15].

Table 2. Classification accuracy [%] shown for different illumination tilt (declination angle from the surface normal) without any scale variation (Wood UTIA BTF). The training sample is illuminated from the surface normal direction.

Illumination tilt [deg]	30	60	75	Avg.
Opponent Gabor	50.1	26.1	14.9	30.8
$LBP_{8,1+8,3}$, color	55.8	25.2	13.6	31.5
2D CAR-KL	83.3	62.9	42.1	**62.8**

University of East Anglia. Detailed comparison for UEA scale variation is displayed in Fig. 4, where we can see classification accuracy significantly increases if scales of training and test samples are closer to each other. The only exception is color histogram features, which cannot recognize the same materials on the same scale due to insufficient robustness to the illumination spectra changes. These conclusions hold for one training sample and six random training samples per class. The 2D CAR-KL features again achieved the best results, where classification accuracy for one training sample starts on 23.1% for half scale factor and goes to 64.9% for the same scale (15% better than alternative features). Opponent Gabor features were slightly better for the highest difference in the scale factor. A similar situation holds for six training samples, where classification accuracy goes from 36.9% to 90.0% for 2D CAR-KL features. However, opponent Gabor features performed better with a significant difference in scale factor (0.5 - 0.7).

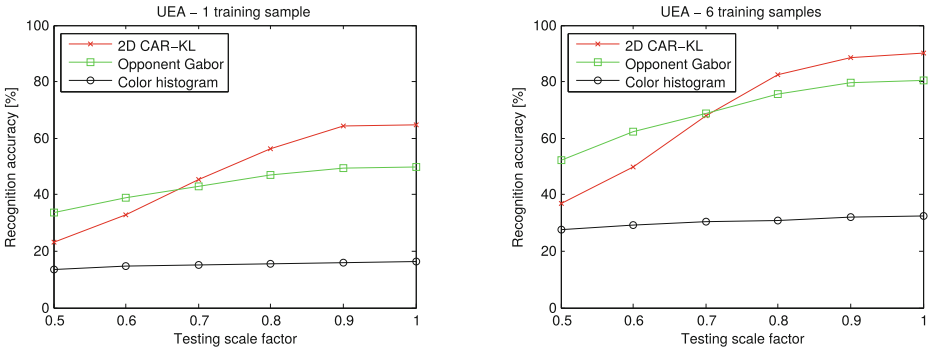

Fig. 4. The illustration of the classification accuracy [%] progresses with decreasing scale differences among training and test sets (UEA). On the left for one training sample and on the right for six training samples per class.

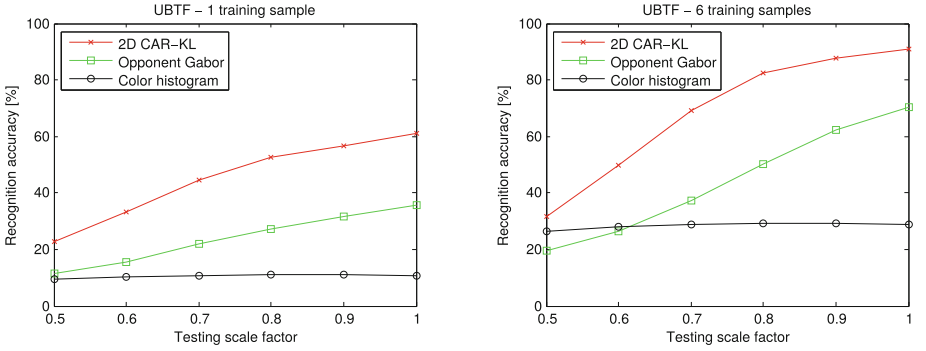

Fig. 5. Classification accuracy [%] progresses with decreasing scale differences among training and test sets (Wood UTIA BTF). On the left for one training sample and on the right for six training samples per class.

Wood UTIA BTF. The detailed comparison of scale variation on Wood UTIA BTF is displayed in Fig. 5. The classification accuracy increases as scales of training and test samples are closer (except for histogram features). The best results were again achieved by 2D CAR-KL features, where classification accuracy for one training sample starts at 22.7% for half scale and goes to 60.9% for the same scale. This improvement is more than 10% better than the opponent Gabor features for all scale factors. A similar situation holds for six training samples, where classification accuracy goes from 31.5% to 91.0% for 2D CAR-KL features, again more than 10% better than opponent Gabor features.

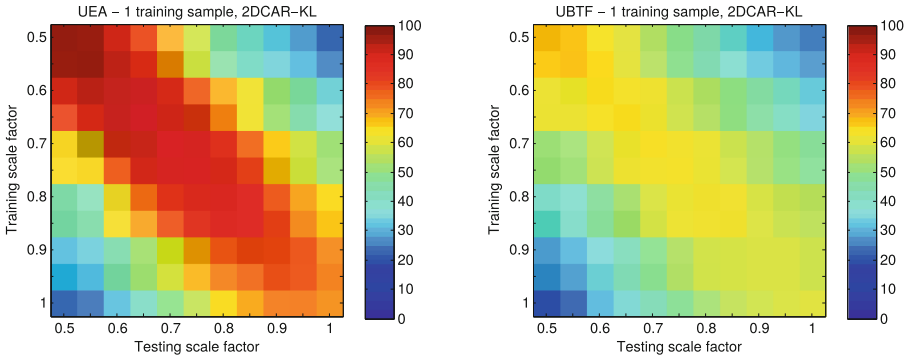

Fig. 6. The classification accuracy [%] for all combinations of scales among training and test sets UEA (left)/Wood UTIA BTF (right), one training sample per class was used.

Across Scales. Figure 6 shows classification accuracy across different training and test scales combinations on UEA and Wood UTIA BTF, with a single training sample (averaged over 10^3 of random selections). As expected, classification accuracy decreases with a more considerable difference in scale factors. It is worth noting that the last rows of images in Fig. 6 correspond to the 2D CAR-KL graphs on the left in Fig. 4 and Fig. 5. Interestingly, recognition accuracy on the diagonal decreases from a scale factor of 0.5 to 1. This decrease may be caused by the fact that images with a scale factor of 0.5 cover a larger area of the original material (although being subsampled), so they contain comprehensive information, and the extracted features can be more discriminative.

Illumination Tilt. The additional experiment utilizes different illumination angles in Wood UTIA BTF and splits classification accuracy for different illumination tilts. The single training sample was fixed to the illumination from a normal surface direction (0-° tilt), and the remaining images were classified. The classification accuracy is averaged for each illumination tilt: 30, 60, and 75° (12, 10, and 12 images). Training and test sets have the same scaling factor 1. The results are displayed in Table 2, where classification accuracy decreases as illumination direction moves further from training sample illumination. The last column's average results roughly correspond to the left graph in Fig. 5 for test scale factor 1. As the scale variation is not present, the results of LBP and opponent Gabor features are comparable.

5 Conclusion

The results indicate that Markovian illumination invariant texture features (2D CAR), based on the Markovian descriptive model, are the most robust textural features for realistic texture classification under the natural conditions when learning and classifying textures differ in scale and illumination properties. The 2D CAR features outperformed alternative tested textural features,

i.e., the Gabor, opponent Gabor, variants of LBP, or color histogram texture features. 2D CAR statistical features are analytically derived from the underlying descriptive textural model and can be efficiently, recursively, and adaptively learned. Their additional advantage is their numerically robust estimation. The method's correct recognition accuracy improvements are between 27% and 44%, compared to the LBP features and up to 25% compared to the opponent Gabor features (the second-best alternative). The worst are color histograms with an accuracy decrease between 35% and 43%. The color Markovian textural features were also successfully applied elsewhere in recognition of wood veneers using a smartphone camera [14], or tree taxonomy categorization based on bark or coniferous tree needles [28]. The presented results apply for recognition with bounded scale variation. The full scale-invariant textural features should be considered for extreme expected scale variation. However, fully invariant features usually lose some discriminability. Thus, each application needs carefully balance invariance to expected variability and discriminability.

References

1. Ahonen, T., Matas, J., He, C., Pietikainen, M.: Rotation invariant image description with local binary pattern histogram Fourier features. In: SCIA, pp. 61–70 (2009). https://doi.org/10.1007/978-3-642-02230-2_7
2. Bell, S., Upchurch, P., Snavely, N., Bala, K.: Material recognition in the wild with the materials in context database. In: Proceedings of the IEEE Conference on Computer Vision and Pattern Recognition, pp. 3479–3487 (2015)
3. Burghouts, G.J., Geusebroek, J.M.: Material-specific adaptation of color invariant features. Patt. Recogn. Lett. **30**, 306–313 (2009). https://doi.org/10.1016/j.patrec.2008.10.005
4. Finlayson, G., Schaefer, G., Tian, G.: The UEA uncalibrated colour image database. Technical Report SYS-C00, School of Information System, University of East Anglia, Norwich, UK (2000)
5. Fu, X., Wei, W.: Centralized binary patterns embedded with image Euclidean distance for facial expression recognition. In: ICNC 2008. Fourth International Conference on Natural Computation 2008, vol. 4, pp. 115–119, October 2008. https://doi.org/10.1109/ICNC.2008.94
6. Gibert, X., Patel, V.M., Chellappa, R.: Material classification and semantic segmentation of railway track images with deep convolutional neural networks. In: 2015 IEEE International Conference on Image Processing (ICIP), pp. 621–625. IEEE (2015)
7. Grigorescu, S.E., Petkov, N., Kruizinga, P.: Comparison of texture features based on Gabor filters. IEEE Trans. Image Process. **11**(10), 1160–1167 (2002)
8. Haindl, M., Havlíček, V.: A multiscale colour texture model. In: Kasturi, R., Laurendeau, D., Suen, C. (eds.) Proceedings of the 16th International Conference on Pattern Recognition, pp. 255–258. IEEE Computer Society, Los Alamitos, August 2002. https://doi.org/10.1109/ICPR.2002.1044676
9. Haindl, M.: Visual data recognition and modeling based on local Markovian models. In: Florack, L., Duits, R., Jongbloed, G., Lieshout, M.C., Davies, L. (eds.) Mathematical Methods for Signal and Image Analysis and Representation, Computational Imaging and Vision, vol. 41, chap. 14, pp. 241–259. Springer, London (2012), https://doi.org/10.1007/978-1-4471-2353-8_14

10. Haindl, M., Filip, J.: Visual Texture. Advances in Computer Vision and Pattern Recognition, Springer-Verlag, London, London, January 2013. https://doi.org/10.1007/978-1-4471-4902-6
11. Haindl, M., Filip, J., Vávra, R.: Digital material appearance: the curse of terabytes. ERCIM News (90), 49–50 (2012). http://ercim-news.ercim.eu/en90/ri/digital-material-appearance-the-curse-of-tera-bytes
12. Haindl, M., Havlíček, V.: A multiresolution causal colour texture model. Lecture Notes in Computer Science, vol. 1876, pp. 114–122 (2000)
13. Haindl, M., Mikeš, S., Kudo, M.: Unsupervised surface reflectance field multi-segmenter. In: Azzopardi, G., Petkov, N. (eds.) Computer Analysis of Images and Patterns. Lecture Notes in Computer Science, vol. 9256, pp. 261–273. Springer International Publishing, September 2015. https://doi.org/10.1007/978-3-319-23192-1_22
14. Haindl, M., Vacha, P.: Wood veneer species recognition using Markovian textural features. In: Azzopardi, G., Petkov, N. (eds.) Computer Analysis of Images and Patterns. Lecture Notes in Computer Science, vol. 9256, pp. 300–311. Springer International Publishing, September 2015. https://doi.org/10.1007/978-3-319-23192-1_25
15. Haindl, M., Vácha, P.: Scale sensitivity of textural features. In: Beltrán-Castañón, C. et al. (eds.) Progress in Pattern Recognition, Image Analysis, Computer Vision, and Applications: 21st Iberoamerican Congress, CIARP 2016, Lima, Peru, 2016, Proceedings. LNCS, vol. 10125, pp. 84–92. Springer International Publishing AG, Gewerbestrasse 11, Cham, CH-6330, Switzerland, November 2017. https://doi.org/10.1007/978-3-319-52277-7_11
16. Han, J., Ma, K.K.: Rotation-invariant and scale-invariant Gabor features for texture image retrieval. Image Vis. Comput. **25**(9), 1474–1481 (2007)
17. Heikkilä, M., Pietikäinen, M., Schmid, C.: Description of interest regions with local binary patterns. Pattern Recogn. **42**(3), 425–436 (2009). https://doi.org/10.1016/j.patcog.2008.08.014
18. Hlaing, C.S., Zaw, S.M.M.: Tomato plant diseases classification using statistical texture feature and color feature. In: 2018 IEEE/ACIS 17th International Conference on Computer and Information Science (ICIS), pp. 439–444. IEEE (2018)
19. Jain, A.K., Healey, G.: A multiscale representation including opponent color features for texture recognition. IEEE Trans. Image Process. **7**(1), 124–128 (1998)
20. Khellah, F.: Texture classification using dominant neighborhood structure. IEEE Trans. Image Process. **20**(11), 3270–3279 (2011). https://doi.org/10.1109/TIP.2011.2143422
21. Li, Z., Liu, G., Jiang, H., Qian, X.: Image copy detection using a robust Gabor texture descriptor. In: Proceedings of the First ACM Workshop on Large-scale Multimedia Retrieval and Mining, pp. 65–72. LS-MMRM 2009. ACM, New York, NY, USA (2009). https://doi.org/10.1145/1631058.1631072
22. Liao, S., Law, M.W.K., Chung, A.C.S.: Dominant local binary patterns for texture classification. IEEE Trans. Image Process. **18**(5), 1107–1118 (2009). https://doi.org/10.1109/TIP.2009.2015682
23. Liu, L., Chen, J., Fieguth, P., Zhao, G., Chellappa, R., Pietikainen, M.: A survey of recent advances in texture representation. arXiv preprint arXiv:1801.10324 (2018)
24. Liu, L., Fieguth, P., Wang, X., Pietikäinen, M., Hu, D.: Evaluation of LBP and deep texture descriptors with a new robustness benchmark. In: European Conference on Computer Vision, pp. 69–86. Springer (2016). https://doi.org/10.1007/978-3-319-46487-9_5

25. Manjunath, B.S., Ma, W.Y.: Texture features for browsing and retrieval of image data. IEEE Trans. Pattern Anal. Mach. Intell. **18**(8), 837–842 (1996). https://doi.org/10.1109/34.531803
26. Nanni, L., Lumini, A., Brahnam, S.: Survey on LBP based texture descriptors for image classification. Expert Syst. Appl. **39**(3), 3634–3641 (2012). https://doi.org/10.1016/j.eswa.2011.09.054
27. Ojala, T., Pietikäinen, M., Mäenpää, T.: Multiresolution gray-scale and rotation invariant texture classification with local binary patterns. IEEE Trans. Pattern Anal. Mach. Intell. **24**(7), 971–987 (2002)
28. Remeš, V., Haindl, M.: Bark recognition using novel rotationally invariant multispectral textural features. Pattern Recogn. Lett. **125**, 612–617 (2019). https://doi.org/10.1016/j.patrec.2019.06.027
29. Roy, S.K., Bhattacharya, N., Chanda, B., Chaudhuri, B.B., Ghosh, D.K.: FWLBP: a scale invariant descriptor for texture classification. arXiv preprint arXiv:1801.03228 (2018)
30. Santini, S., Jain, R.: Similarity measures. IEEE Trans. Patt. Anal. Mach. Intell. **21**(9), 871–883 (1999)
31. Shivashankar, S., Kudari, M., Hiremath, P.S.: Galois field-based approach for rotation and scale invariant texture classification. Int. J. Image, Graph. Signal Process. (IJIGSP) **10**(9), 56–64 (2018)
32. Sidiropoulos, G.K., Ouzounis, A.G., Papakostas, G.A., Sarafis, I.T., Stamkos, A., Solakis, G.: Texture analysis for machine learning based marble tiles sorting. In: 2021 IEEE 11th Annual Computing and Communication Workshop and Conference (CCWC), pp. 0045–0051. IEEE (2021)
33. Simon, P., Uma, V.: Review of texture descriptors for texture classification. In: Data Engineering and Intelligent Computing, pp. 159–176. Springer (2018). https://doi.org/10.1007/978-981-10-3223-3_15
34. Stricker, M.A., Orengo, M.: Similarity of color images, vol. 2420, pp. 381–392. SPIE (1995). https://doi.org/10.1117/12.205308
35. Vácha, P., Haindl, M.: Texture recognition using robust Markovian features. In: Salerno, E. et al. (eds.) Computational Intelligence for Multimedia Understanding, Lecture Notes in Computer Science, vol. 7252, pp. 126–137. Springer, Berlin/Heidelberg (2012). https://doi.org/10.1007/978-3-642-32436-9_11
36. Vácha, P., Haindl, M., Suk, T.: Colour and rotation invariant textural features based on Markov random fields. Pattern Recogn. Lett. **32**(6), 771–779 (2011). https://doi.org/10.1016/j.patrec.2011.01.002
37. Varma, M., Zisserman, A.: A statistical approach to material classification using image patch exemplars. IEEE Trans. Pattern Anal. Mach. Intell. **31**(11), 2032–2047 (2009). https://doi.org/10.1109/TPAMI.2008.182
38. Veerashetty, S., Patil, N.B.: Novel LBP based texture descriptor for rotation, illumination and scale invariance for image texture analysis and classification using multi-Kernel SVM. Multimedia Tools Appl. **79**(15), 9935–9955 (2020)
39. Yang, P., Zhang, F., Yang, G.: Fusing DTCWT and LBP based features for rotation, illumination and scale invariant texture classification. IEEE Access **6**, 13336–13349 (2018)
40. Zhang, B., Gao, Y., Zhao, S., Liu, J.: Local derivative pattern versus local binary pattern: face recognition with high-order local pattern descriptor. IEEE Trans. Image Process. **19**(2), 533–544 (2010)